New Journal of Physics
The open access journal at the forefront of physics

Deutsche Physikalische Gesellschaft DPG
IOP Institute of Physics

Published in partnership with: Deutsche Physikalische Gesellschaft and the Institute of Physics

OPEN ACCESS

RECEIVED
3 April 2020

REVISED
11 July 2020

ACCEPTED FOR PUBLICATION
27 July 2020

PUBLISHED
27 August 2020

PAPER

Magnetotransport of Weyl semimetals with tilted Dirac cones

Anirban Kundu, Zhuo Bin Siu, Hyunsoo Yang and Mansoor B A Jalil[1]

Department of Electrical and Computer Engineering, National University of Singapore, 4 Engineering Drive 3, 117576 Singapore
[1] Author to whom any correspondence should be addressed.

E-mail: elembaj@nus.edu.sg

Keywords: condensed matter physics, mesoscopic physics, topological material, Weyl semimetal, Dirac semimetal

Supplementary material for this article is available online

Abstract

Weyl semimetals (WSM) exhibit chiral anomaly in their magnetotransport due to broken conservation laws. Here, we analyze the magnetotransport of WSM in the presence of the time-reversal symmetry-breaking tilt parameter. The analytical expression for the magnetoconductivity is derived in the small tilt limit using the semiclassical Boltzmann equation. We predict a planar Hall current which flows transverse to the electric field and in the plane containing magnetic and electric fields and scales linearly with the tilt parameter. A tilt-induced transverse conductivity is also present in the case where the electric and magnetic fields are parallel to each other, a scenario where the conventional Hall current completely vanishes.

1. Introduction

A Weyl semimetal (WSM) state in topological systems with broken time-reversal and/or inversion symmetry can be understood by the availability of the low energy quasiparticles called Weyl Fermions (WF) with linear in momentum dispersion near the crossing point of two non-degenerate bands in momentum space known as Weyl point (WP) [1–3]. Although the concept of WF was first introduced in relativistic field theory, it has never been observed in the systems of elementary particles, and has only very recently been realized in a condensed matter systems as an excitation of quasi-particles [4–6]. The essential properties of WPs are: the presence of pairs of opposite chiralities connected by Fermi arcs on the surface and the zero-sum of chiralities over all the WPs in the Brillouin zone, according to the Nielsen–Ninomiya theorem [7]. The chirality χ of a WP is defined by the integration of Berry curvature $\mathbf{\Omega_k}$ ($\mathbf{\Omega_k} = \nabla \times \mathbf{A_k}$ with $\mathbf{A_k} = i\langle u_\mathbf{k}|\nabla_\mathbf{k} u_\mathbf{k}\rangle$, where $|u_\mathbf{k}\rangle$ is the Bloch wave function) over a closed surface around that WP in momentum space ($\oint \mathbf{ds} \cdot \mathbf{\Omega_k} = 2\pi\chi$ where, $\chi = \pm 1, \pm 2, \ldots$.).

In the presence of external electric and magnetic fields the conservation of the number of WFs with particular chirality is broken, a phenomenon known as chiral anomaly. The WSMs are distinctive from other metals/semi-metals because the chiral anomaly can lead to unusual magneto-transport phenomena [8]. The observation of negative magneto-conductivity has also been attributed to the phenomenon of chiral anomaly [9–14] although recently it has been argued that other physical process may also contribute to the magneto-conductivity [15, 16].

In this manuscript, we study the electron transport in WSM where the Dirac cones are tilted in momentum space. Such a tilted WSM can be described by an additional anisotropy term in the Hamiltonian for electrons near a WP as follows [17],

$$H_\chi = \chi v_\mathrm{F} \boldsymbol{\sigma} \cdot \mathbf{k} + I\mathbf{w}_\chi \cdot \mathbf{k}, \tag{1}$$

where $\chi = \pm 1$ indicates the chirality of each Weyl node, the components of $\boldsymbol{\sigma}$ are the Pauli matrices and I is the 2×2 identity matrix, $\mathbf{k}$ is the wave vector, the vector $\mathbf{w}_\chi$ represents the dispersion tilt and v_F is the Fermi velocity. The first term in equation (1) represents the Hamiltonian of electrons near the WPs when the time reversal symmetry (TRS) is broken and the second term including tilt $\mathbf{w}_\chi$ also breaks the TRS. Note that in WSMs where the Weyl nodes are separated by broken inversion symmetry but related to one

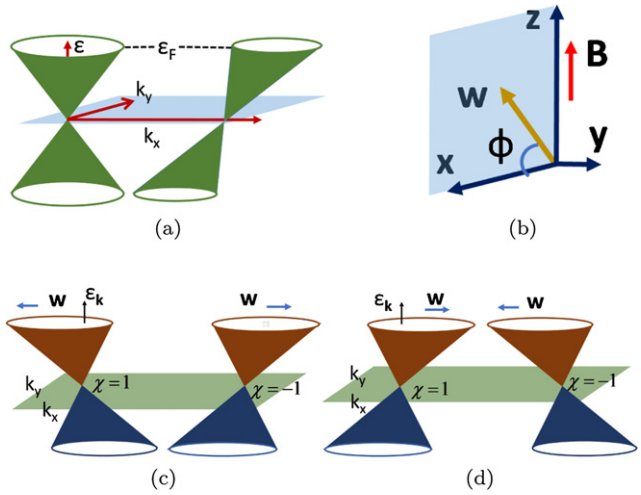

Figure 1. (a) Dispersion relation for the non-tilted (left) and tilted (right) WSM. (b) The z-axis is parallel to the magnetic field while the tilt vector $\mathbf{w}_\chi = \mathbf{w}$ lies on the x–z plane with an angle ϕ from the x-axis. (c) and (d), A pair of Dirac cones are tilted (c) towards each other, and (d) away from each other.

another by the time reversal operation (the case which we will discuss later), the tilt term will then be solely responsible for breaking the TRS. The energy eigenvalues are given by $\lambda_{k_\chi} = (\hbar \mathbf{w}_\chi \cdot \mathbf{k} + \chi \hbar v_{\mathrm{F}} \mathrm{k}))$ and the corresponding group velocity is $\mathbf{v}_{\mathbf{k}}^{\chi} = (\mathbf{w}_\chi + \chi v_{\mathrm{F}} \hat{\mathrm{k}})$ (where $\hat{\mathrm{k}}$ is the unit vector along $\mathbf{k}$ and v_{F} the Fermi velocity). If the value of tilt $|\mathbf{w}_\chi| < v_{\mathrm{F}}$ then the WSMs are sub-grouped as type-I WSM and when $|\mathbf{w}_\chi| > v_{\mathrm{F}}$ then the WSMs are sub-grouped as type-II WSM. A non-tilted and tilted dispersion relation in WSM is shown in the schematic diagram in figure 1(a). Type-II WSM phase has been observed in a range of materials such as $MoTe_2$, WTe_2, LaAlGe [18–21] and transport related phenomena in these materials have been addressed in several studies [22–27].

Transport studies of tilted Weyl semimetals have been done recently such as anomalous Nernst effect [28–30], optical response to circularly polarized light [31], conductance modulation in the presence of tilt [32], planar Hall effect (PHE) [33] and tilt-dependent magneto-transport [34, 35]. The anomalous transport properties of a WSM p–n–p heterojunction device in the presence of tilt have been studied in references [36, 37]. Using Boltzmann transport it has been predicted that both the chiral anomaly and non-trivial Berry curvature effects leads to the PHE in Weyl semimetals [38] and very recently, PHE in half Heusler Weyl semimetal GdPtBi has been attributed to a strong Berry curvature effect [39].

Although in the above studies several transport properties have been investigated in the presence of tilt, a detailed study of the role of the tilt and how does it manifests itself on the transport properties is still not understood very well. We try to address this issue by considering different configurations of tilt in the WSM systems. In particular, we study a type-I WSM system with tilt direction ($\mathbf{w}_\chi$) to be chosen arbitrarily and we consider two scenarios, with Dirac cones for a pair of Weyl nodes to be tilted along the same direction and opposite directions. Both the longitudinal and transverse conductivities are calculated using the Boltzmann transport equation while treating the tilt as a parameter with a small magnitude and oriented some arbitrary direction. We show that the PHE can be generated only when the tilts for a pair of Weyl nodes are tilted in the opposite directions and more importantly it can be tuned with the tilt direction and magnitude. Our manuscript is arranged as follows: in section 2 we present the general framework of the semiclassical Boltzmann model to calculate the current density up to the second orders in the B field. In section 3 we present the analytical expression for the conductivity in the small-tilt regime. We also perform numerical calculations for arbitrary tilt value in the case of both type-I and type-II WSM (results of the latter are presented in more detail in the supplemental) (http://stacks.iop.org/NJP/22/083081/mmedia) and verify the analytical results in the limit of small tilt. The anisotropy of the WSM conductivity with respect to the magnetic field and tilt directions is also presented. We conclude in section 4.

2. Method

We apply the semiclassical Boltzmann transport model where we study the dynamics of the wave-packet under the assumption of a small external magnetic and electric fields where the separation between Landau levels can be neglected and where it is valid to use the semiclassical approach [40]. We begin with the standard procedure to calculate the Boltzmann's distribution function for a system with non-zero Berry

curvature under the application of external electric and magnetic field. The presence of Berry curvature $\mathbf{\Omega_k}$ in the WSMs provides a correction to the phase space volume in the case of adiabatic transport, as shown in [41, 42]. In the presence of electric ($\mathbf{E}$) and magnetic field ($\mathbf{B}$) the semiclassical equations of motion of the wave-packet are modified as follows [41],

$$\dot{\mathbf{r}} = \left(1 + \frac{e}{\hbar}\mathbf{\Omega_k}\cdot\mathbf{B}\right)^{-1}\left[\boldsymbol{v}_\mathbf{k} + e\mathbf{E}\times\mathbf{\Omega_k} + \frac{e}{\hbar}(\mathbf{\Omega_k}\cdot\boldsymbol{v}_\mathbf{k})\mathbf{B}\right],$$
$$\hbar\dot{\mathbf{k}} = \left(1 + \frac{e}{\hbar}\mathbf{\Omega_k}\cdot\mathbf{B}\right)^{-1}\left[e\mathbf{E} + \frac{e}{\hbar}\boldsymbol{v}_\mathbf{k}\times\mathbf{B} + \frac{\mathrm{e}^2}{\hbar}(\mathbf{E}\cdot\mathbf{B})\mathbf{\Omega_k}\right], \tag{2}$$

where, the energy of the wave packet is given by, $\epsilon_k = (\lambda_\mathbf{k} - \mathbf{m_k}\cdot\mathbf{B})$. Here, $\lambda_\mathbf{k}$ is the energy dispersion of the electron corresponding to the band considered (this is given in the Introduction for WSMs with tilt) and the second term is the correction due to the orbital magnetization of the wave-packet [42]. Then, the group velocity of the electron is given by $\boldsymbol{v}_\mathbf{k} = \partial\epsilon_\mathbf{k}/\hbar\partial\mathbf{k} = \partial(\lambda_\mathbf{k})/\hbar\partial\mathbf{k} - \partial(\mathbf{m_k}\cdot\mathbf{B})/\hbar\partial\mathbf{k}$. To evaluate the distribution $f(\mathbf{r},\mathbf{k},t)$ we consider the Boltzmann's equation,

$$\frac{\partial f(\mathbf{r},\mathbf{k},t)}{\partial t} + \dot{\mathbf{r}}\cdot\frac{\partial f(\mathbf{r},\mathbf{k},t)}{\partial\mathbf{r}} + \dot{\mathbf{k}}\cdot\frac{\partial f(\mathbf{r},\mathbf{k},t)}{\partial\mathbf{k}} = I_{\mathrm{coll}}\left\{f(\mathbf{r},\mathbf{k},t)\right\}, \tag{3}$$

where $I_{\mathrm{coll}}\left\{f(\mathbf{r},\mathbf{k},t)\right\}$ is the collision integral. We solve for the change in the distribution function δf for a uniform system under steady-state condition, i.e., ignoring the time and space dependence in the above equation, and apply the relaxation time approximation, i.e., $I_{\mathrm{coll}}\left\{f(\mathbf{r},\mathbf{k},t)\right\} = \delta f(\mathbf{r},\mathbf{k},t)/\tau(\mathbf{k})$, where, $\tau(\mathbf{k})$ is the relaxation time. The relaxation time $\tau(\mathbf{k})$ is in general k-dependent where the specific dependence on $\mathbf{k}$ can be derived from the scattering potential in the sample. However, as most of the contribution to the conductivity is obtained after angular integration over the FS and occurs at energy well away from the Weyl point (note that the conductivity goes to zero at the Weyl point, where the FS shrinks to a point), unless there is a very strong anisotropy or directional dependence of $\tau(\mathbf{k})$ on $\mathbf{k}$, the resulting conductivity would not be modified significantly. So, mainly to avoid analytical complexity, we have adopted the constant relaxation time approximation, i.e., τ being independent of $\mathbf{k}$, which is also adopted by previous theoretical works on the semiclassical transport formalism in WSMs, as in references [28, 30, 38, 40]. Assuming the second-order derivative of the distribution function to be negligible, the change in the distribution function is evaluated from equations (2) and (3) as,

$$\delta f(\mathbf{r},\mathbf{k},t) = -\tau\left(1 + \frac{e}{\hbar}\mathbf{\Omega_k}\cdot\mathbf{B}\right)^{-1}\hbar^{-1}\left(e\mathbf{E} + \frac{\mathrm{e}^2}{\hbar}(\mathbf{E}\cdot\mathbf{B})\,\mathbf{\Omega_k}\right)\cdot\mathbf{v_k}\left(\partial f^0/\partial\epsilon\right), \tag{4}$$

where ϵ is the electron energy and f^0 is the equilibrium distribution function which usually can be replaced by Fermi function. As we are interested in the Berry-curvature induced effect only, we neglect the effect of Lorentz force (see the second line of equation (2)) which produces the conventional Hall current. The expression of current density is given by, $\mathbf{j} = \left(e/8\pi^3\right)\int \mathrm{d}\mathbf{k}\,(1 + (e/\hbar)\mathbf{\Omega_k}\cdot\mathbf{B})^{-1}\dot{\mathbf{r}}\delta f(\mathbf{k})$ and using the above results for a single Weyl node we obtain,

$$\mathbf{j} = \frac{e\tau}{4\pi^3\hbar}\int \mathrm{d}\epsilon\frac{\partial f^0}{\partial\epsilon}\int \mathrm{d}S\frac{1}{(1 + \frac{e}{\hbar}\mathbf{\Omega_k}\cdot\mathbf{B})|\mathbf{v_k}|}\left[(e\mathbf{E}\cdot\mathbf{v_k})\mathbf{v_k} + \frac{\mathrm{e}^2}{\hbar}(\mathbf{E}\cdot\mathbf{B})\right.$$
$$\left.\times\left((\mathbf{\Omega_k}\cdot\mathbf{v_k})\mathbf{v_k} + \frac{e\mathbf{B}}{\hbar^2}(\mathbf{\Omega_k}\cdot\mathbf{v_k})^2\right) + \frac{\mathrm{e}^2\mathbf{B}}{\hbar}(\mathbf{E}\cdot\mathbf{v_k})(\mathbf{\Omega_k}\cdot\mathbf{v_k})\right], \tag{5}$$

where S is the area of the constant energy surface. The current density above originates due to the imbalance between the particles numbers in the right-handed and left-handed valleys in the presence of the external electric and magnetic fields (i.e., the phenomenon of chiral anomaly), as discussed in reference [40]. Next, we expand $\mathbf{j}$ to various orders of magnetic field as follows:
$\left(1 + (e/\hbar)\mathbf{\Omega_k}\cdot\mathbf{B}\right)^{-1} = 1 - (e/\hbar)\mathbf{\Omega_k}\cdot\mathbf{B} + (e/\hbar)^2(\mathbf{\Omega_k}\cdot\mathbf{B})^2 + \mathcal{O}\left(|\mathbf{B}|^3\right)$ and so that one can express the current density as, $\mathbf{j} = \mathbf{j}^{(0)} + \mathbf{j}^{(1)} + \mathbf{j}^{(2)} + \cdots$ where the numbers in the superscript represent the orders of the magnetic field. Next, we substitute the expression of the Berry curvature in WSM as given by, $\mathbf{\Omega_k} = -\chi\left(1/2\mathrm{k}^3\right)\mathbf{k}$, and, we define $\mathbf{v_k} = \partial(\lambda_\mathbf{k})/\hbar\partial\mathbf{k}$ and $\mathbf{v}_\mathbf{k}^{\mathrm{orb}} = \partial(\mathbf{m_k}\cdot\mathbf{B})/\hbar\partial\mathbf{k}$ where the orbital magnetic moment $\mathbf{m_k} = -\chi v_\mathrm{F}\mathrm{k}\left(1/2\mathrm{k}^3\right)\mathbf{k}$ [22, 43], into the above expression of current density and obtain for a single valley,

$$\mathbf{j}^{(0)} = \sigma_0\int \mathrm{d}\epsilon\frac{\partial f^0}{\partial\epsilon}\int\frac{\mathrm{d}S}{k_F^2|\mathbf{v_k}|v_\mathrm{F}}(\mathbf{E}\cdot\mathbf{v_k})\,\mathbf{v_k}, \tag{6}$$

$$\mathbf{j}^{(1)} = \sigma_0 c_b \int \mathrm{d}\epsilon \frac{\partial f^0}{\partial \epsilon} \int \frac{\mathrm{d}S}{k_F^2 |\mathbf{v_k}| v_\mathrm{F}} \left[\mathbf{B}\,(\mathbf{E}\cdot\mathbf{v_k})\,(\mathbf{\Omega_k}\cdot\mathbf{v_k}) + (\mathbf{E}\cdot\mathbf{B})\,(\mathbf{\Omega_k}\cdot\mathbf{v_k})\,\mathbf{v_k} - (\mathbf{\Omega_k}\cdot\mathbf{B})\,(\mathbf{E}\cdot\mathbf{v_k})\,\mathbf{v_k} - (\mathbf{E}\cdot\mathbf{v_k})\,\mathbf{v_k^{orb}}\right], \tag{7}$$

$$\begin{aligned}\mathbf{j}^{(2)} = \sigma_0 c_b^2 \int \mathrm{d}\epsilon \frac{\partial f^0}{\partial \epsilon} \int \frac{\mathrm{d}S}{k_F^2 |\mathbf{v_k}| v_\mathrm{F}} \Big[&(\mathbf{\Omega_k}\cdot\mathbf{B})^2\,(\mathbf{E}\cdot\mathbf{v_k})\,\mathbf{v_k} - \mathbf{B}\,(\mathbf{E}\cdot\mathbf{v_k})\,(\mathbf{\Omega_k}\cdot\mathbf{B})\,(\mathbf{\Omega_k}\cdot\mathbf{v_k}) + \mathbf{B}\left(\mathbf{E}\cdot\mathbf{v_k^{orb}}\right)(\mathbf{\Omega_k}\cdot\mathbf{v_k}) \\ &+ (\mathbf{E}\cdot\mathbf{B})\left(\mathbf{\Omega_k}\cdot\mathbf{v_k^{orb}}\right)\mathbf{v_k} - (\mathbf{\Omega_k}\cdot\mathbf{B})\left(\mathbf{E}\cdot\mathbf{v_k^{orb}}\right)\mathbf{v_k} + (\mathbf{E}\cdot\mathbf{B})\left(\mathbf{B}(\mathbf{\Omega_k}\cdot\mathbf{v_k})^2\frac{\mathbf{v_k}}{|\mathbf{v_k}|} - (\mathbf{\Omega_k}\cdot\mathbf{v_k})\,(\mathbf{\Omega_k}\cdot\mathbf{B})\,\mathbf{v_k}\right)\Big].\end{aligned} \tag{8}$$

In the above, $c_b = e\hbar v_\mathrm{F}^2/\epsilon_\mathrm{F}^2$ and $\sigma_0 = \mathrm{e}^2\tau\epsilon_\mathrm{F}^2/4\pi^3\hbar^3 v_\mathrm{F}$. Note that the first and second-order terms in B arise entirely as a result of the non-zero Berry curvature. Now, to evaluate the current density one needs to integrate over energy and momentum. We consider a model Hamiltonian given in equation (1) with linear dispersion which describes a tilted WSM (for both type-I and type-II). For the type-I case, we calculate the current density in two different ways: (i) we first assume a small tilt limit and obtain the analytical expression of the current density to the first order in the tilt vector **w**; (ii), we calculate the current density numerically for arbitrary value of tilt, and compare the results with the analytical expression obtained in the small tilt limit. For type-II WSM, we only perform the numerical calculation and present the results in the supplemental.

3. Tilted WSM

Small tilt limit ($|\mathbf{w}_\chi| \ll v_\mathrm{F}$). For small tilt, we expand equations (6)–(8) to the first order in $\mathbf{w}_\chi$ using $|\mathbf{v}_\mathbf{k}^\chi| \approx \chi v_\mathrm{F} + (\hat{\mathrm{k}}\cdot\mathbf{w}_\chi) + \mathcal{O}\left(|\mathbf{w}_\chi|^2\right)$. The presence of a finite tilt to the energy dispersion changes the shape of the Fermi surface (FS). However, in the small tilt limit, one can neglect this change and assume the shape of the FS to be spherical. We also consider the low-temperature limit such that we can approximate the distribution function f^0 to be the step function $\theta(\epsilon - \epsilon_\mathrm{F})$ and consequently $\partial f^0/\partial\epsilon$ can be replaced by a Dirac delta function given by $\delta(\epsilon - \epsilon_\mathrm{F})$ (note that most of the experimental transport measurements on WSMs are done at low temperatures at which this approximation is valid). Without loss of any generality, we choose the z-axis to be aligned along the magnetic field ($\mathbf{B} = B\hat{z}$) and that $\mathbf{w}_\chi$ and **B** lie in the same plane (figure 1(b)). Choosing the plane to be the x–z plane, we write, $\mathbf{w}_\chi = \mathrm{w}_x^\chi\hat{x} + \mathrm{w}_z^\chi\hat{z}$ (w_x^χ and w_z^χ are the components of tilt and $\hat{x}$ and $\hat{z}$ are unit vectors along x and z-axis). Under the above assumptions, we calculate the current densities for a pair of Weyl nodes with opposite chirality to the first order in tilt and to the various orders in magnitude of the magnetic field B. While doing so we considered two distinct cases: (I) the tilt changes sign between the valleys with opposite chirality i.e. $\mathbf{w}_\chi = \chi\mathbf{w}$, and (II) the sign of the tilt remains unchanged in the two valleys i.e. $\mathbf{w}_\chi = \mathbf{w}$.

Case (a). In the small tilt limit, the current density can be evaluated analytically derived from the integrals in equations (6)–(8) with **E** is chosen to be along $\|(\hat{x} + \hat{z})$. The current density of different orders in B is given by (see the supplemental information for more details on the derivation):

$$\mathbf{j}^{(0)} = \frac{8\pi}{3}\sigma_0\mathbf{E}, \tag{9}$$

$$\mathbf{j}^{(1)} = \frac{4\pi}{15}\sigma_0 c_b\left[27\,(\mathbf{E}\cdot\mathbf{B})\,\mathbf{w} + 27\,(\mathbf{E}\cdot\mathbf{w})\,\mathbf{B} + 7(\mathbf{w}\cdot\mathbf{B})\mathbf{E}\right], \tag{10}$$

$$\mathbf{j}^{(2)} = 2\pi\sigma_0 c_b^2\left(\frac{1}{3}\,(\mathbf{E}\cdot\mathbf{B})\,\mathbf{B} + |\mathbf{B}|^2\frac{1}{15}\mathbf{E}\right). \tag{11}$$

Interestingly, the first-order term is non-vanishing only in the presence of tilt, while the zeroth and second-order terms are independent of the tilt. This linear dependence of the conductivity on the tilt has been predicted before by reference [43]. In our case, we adopt the conventional assumption that intra-valley scattering is the dominant process, and we neglect the inter-valley contribution [44]. In general, the WPs are well-separated in the momentum space by a vector **Q**, whose magnitude is much larger than the Fermi wavevector. Hence the relaxation rate for two intra-valley and inter-valley processes are such that $1/\tau_\mathrm{intra} \gg 1/\tau_\mathrm{inter}$. As a consequence, the inter-valley scattering term in the Boltzmann equation can be neglected, an assumption which was also assumed previously by references [28, 44–46]. This tilt dependence can be understood from the following argument. The anisotropic tilt appears in the integrals in equations (6)–(8) because of the dependence of the group velocity $\mathbf{v_k}$ on tilt. In the case of both $\mathbf{j}^{(0)}$ and $\mathbf{j}^{(2)}$ all the terms in the integral are even in **k** in absence of tilt. However, in the presence of the dispersion tilt, these terms (to the first order in tilt) become odd in **k** i.e. the integrals change sign as one goes from **k** to $-\mathbf{k}$, and, as a consequence, vanish after integration over the FS (which is taken to be spherical). Conversely,

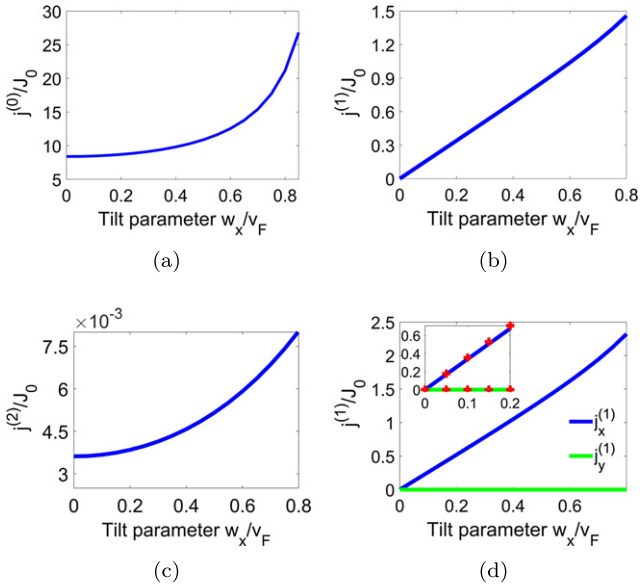

Figure 2. (a)–(c), Plot of longitudinal components of current density $\mathbf{j}^{(0)}$, $\mathbf{j}^{(1)}$ and $\mathbf{j}^{(2)}$ with respect to x-component of tilt (w_x) when electric field $\mathbf{E} \parallel (\hat{x}+\hat{z})$. We use $J_0 = \sigma_0|\mathbf{E}|$. (d) Plot of x and y components of $\mathbf{j}^{(1)}$ with respect to x-component of tilt w_x when $\mathbf{E}\|\mathbf{B}\|\hat{z}$. Inset: Comparison with the analytical results (red circle), which are in close agreement with the numerical results at the small tilt limit.

for $\mathbf{j}^{(1)}$, all the terms in the current integral up to the first order in tilt are even in $\mathbf{k}$, and hence integration over the FS is not necessarily zero.

To understand the dependence of tilt on the current, we consider the implications of equation (10). We consider two particular cases, first, $\mathbf{E} \parallel \mathbf{B}$ i.e. the measurement set-up for longitudinal magnetoconductivity and second, $\mathbf{E} \perp \mathbf{B}$ i.e. the usual Hall measurement set-up. In the first case, i.e. for $\mathbf{E} \parallel \mathbf{B} \parallel \hat{z}$, we obtain,

$$\mathbf{j}^{(1)} = \sigma_0 c_b \frac{4\pi}{15 v_\mathrm{F}} \left(27 B\mathbf{w} + 34 \mathrm{w}_z \mathbf{B}\right) E. \tag{12}$$

Clearly, the current density has components not only along the direction of the magnetic field but also along the tilt directions. As a consequence, we have current transverse to the external electric field in the x–z plane (the plane containing the tilt vector), i.e., $\mathbf{j}_x^{(1)} = \hat{x}\left(4\pi/15 v_\mathrm{F}\right)\sigma_0 c_b \left(27|\mathbf{E}|B\mathrm{w}_x\right)$ but no transverse current density perpendicular to that plane, i.e., $\mathbf{j}_y^{(1)} = 0$.

Note that in the case of the longitudinal magneto-conductivity set up i.e. when $\mathbf{E} \parallel \mathbf{B}$, one usually obtains only the longitudinal component of current density since the Lorentz force is zero. However, in this case, we obtain non-zero transverse conductivity in the presence of tilt and Berry curvature. This unusual transverse signal should be readily measurable in this measurement set-up as one does not need to take into account the background Lorentz force induced Hall current. The tilt is a material-specific parameter whose direction and magnitude can, in principle, be determined from the band structure. If these tilt parameters are known, then our model can provide a prediction of the Berry curvature induced current. Numerically, from the plot in figure 2(d), we predict a planar Hall (PH) conductivity of 19.46 $\Omega^{-1}\,\mathrm{m}^{-1}$ for a tilt value $\mathrm{w}_x = 0.1$ along the x-direction for type-I WSM, and 14.21 $\Omega^{-1}\,\mathrm{m}^{-1}$ for a tilt $\mathrm{w}_x = 1.6$ for type-II WSM (plot is in the supplemental).

Similarly, for the $\mathbf{E} \perp \mathbf{B}$ set-up, we derive the analytical expression for current in the small tilt limit to be,

$$\mathbf{j}^{(1)} = \frac{4\pi}{15}\sigma_0 c_b \left[27\left(\mathbf{E}\cdot\mathbf{w}\right)\mathbf{B} - 7\left(\mathbf{B}\cdot\mathbf{w}\right)\mathbf{E}\right]. \tag{13}$$

From above, we see that the current density has no component along the conventional Hall direction (i.e. parallel to $\mathbf{E}\times\mathbf{B}$). However, there is a non-zero planar Hall (PH) signal. In general, the PH effect is defined as the transverse current in the plane containing the electric and magnetic fields (i.e. along $\mathbf{E}\times(\mathbf{E}\times\mathbf{B})$ direction) when these fields are not parallel to each other. In our particular scenario, the PH current is parallel to $\mathbf{B}$ and is given by $\mathbf{j}_\mathrm{PH}^{(1)} = \left(4\pi/15 v_\mathrm{F}\right)\sigma_0 c_b 27\left(\mathbf{E}\cdot\mathbf{w}\right)\mathbf{B}$.

Arbitrary tilt strength. The analytical current density expressions derived in the previous section holds only in the small tilt limit. For arbitrarily large tilt strength, we calculate the conductivity numerically based on equations (6)–(8). In our numerical calculations, we assume the characteristic collision time to be $\tau = 10^{-13}$ s [14, 47] and Fermi energy $\epsilon_\mathrm{F} = 0.1$ eV. We set the magnetic field to be 3 T, electric field to be

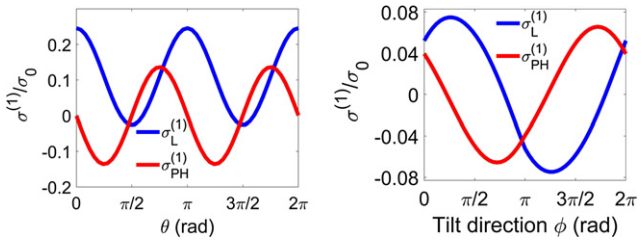

Figure 3. Plot of longitudinal (blue) and PH (red) components of $\mathbf{j}^{(1)}$ with respect to (a) θ, the angle between the electric and magnetic fields, and (b) with respect to the tilt direction ϕ.

10^8 V m^{-1} and the temperature $T = 30$ K. With these parameter values we have $\sigma_0 = 52.84\,\Omega^{-1}\,\mathrm{m}^{-1}$. In figures 2(a)–(c), we plot the longitudinal components of the zeroth, first and second-order terms of the current density as a function of the dispersion tilt in the x-direction, i.e., w_x ($w_z = 0$) when the electric field direction is chosen arbitrarily to be $\mathbf{E} \parallel (\hat{x} + \hat{z})$ (i.e. $\mathbf{E}$ lies in the plane containing $\mathbf{w}$ and $\mathbf{B}$). At small tilt, the zeroth $j^{(0)}$ and second-order term $j^{(2)}$ does not change appreciably with the tilt, confirming our analytical prediction that the two terms are independent of the tilt at the small tilt limit (equation (9) and (11)). However, at sufficiently large tilt ($|\mathbf{w}|/v_\mathrm{F} > 0.2$), the response of those terms to the tilt becomes non-linear. By contrast, the first-order term $j^{(1)}$ varies linearly with the tilt parameter w_x even at large tilt, a response that is in line with the analytical result of equation (10).

Note that all the various orders of current density show an increasing trend with the tilt parameter. A possible reason for this increase of current density is due to the fact that the magnitude of the group velocity $\mathbf{v_k}$ and the area of the FS both increase with the tilt strength. Although the addition of a tilt term in the Hamiltonian does not change the topological properties of the WSMs, it does change the energy dispersion and as a consequence the shape of the FS. For a type-I WSM, the shape of FS is ellipsoid where the axis of the ellipsoid is determined by the tilt direction while for type-II, the shape becomes hyperboloid. As the total current density is calculated by integrating over the FS, the shape and size of the FS have an influence on the current density. The effect of the FS geometry is even more prominent in the case of type-II WSM (this is discussed at the end of this section based on results given in the supplemental).

Next, we evaluate numerically the transverse current in the longitudinal magneto-conductivity setup, i.e., $\mathbf{E} \parallel \mathbf{B} \parallel \hat{z}$. In figure 2(d), we plot the perpendicular components of $\mathbf{j}^{(1)}$ corresponding to this set up, both in the in-plane (x–z plane) and out-of-plane directions, as a function of the tilt parameter w_x. In the inset, the numerical results are compared with the analytical prediction of equation (12), showing good agreement at the small tilt values. It can be seen that the in-plane transverse component of current density increases linearly with w_x while the out-of-plane component is zero, both trends of which match that of the analytical form in equation (12).

The presence of the in-plane transverse current in figure 2(d) even in the longitudinal set up where the $\mathbf{E}$ and $\mathbf{B}$ fields are parallel to each other can be understood in terms of the group velocity $\mathbf{v_k}$ in equation (7). In the absence of tilt $\mathbf{v_k} \parallel \mathbf{k} \parallel \mathbf{\Omega_k}$, and, thus the second and third terms are odd in $\mathbf{k}$ as a consequence of which the integration over FS is zero for those terms, resulting in the current being parallel to $\mathbf{B}$. However at finite tilt, $|\mathbf{v_k}| = v_\mathrm{F}\hat{\mathrm{k}} + \mathbf{w}$, and as a result a component of the current density along the tilt direction appears. In our case, we considered $\mathbf{w} = \mathrm{w}_x\hat{x}$ and thus we obtain a transverse current in the x-direction, which is also in accordance with our calculation in equation (12).

Next, we consider the longitudinal and PH current densities under varying the angle θ between the electric and magnetic fields, under varying tilt direction (denoted by ϕ). We express the tilt vector as $\mathbf{w} = |\mathbf{w}|(\cos\,\phi\,\hat{x} + \sin\,\phi\,\hat{z})$, where ϕ is the angle between the tilt vector and the x-axis. The electric field is chosen to lie on the x–z plane, i.e., $\mathbf{E} = |\mathbf{E}|(\sin\,\theta\,\hat{x} + \cos\,\theta\,\hat{z})$. Substituting the expressions for $\mathbf{w}$ and $\mathbf{E}$ into equation (10), the angular dependence of the longitudinal and PH conductivities at the small tilt is given as,

$$\sigma^{(1)}_\mathrm{L} = \frac{4\pi B|\mathbf{w}|}{15v_\mathrm{F}}\,(27\ \sin(2\theta+\phi) + 34\ \sin\ \phi)\,, \tag{14}$$

and

$$\sigma^{(1)}_\mathrm{PH} = \frac{4\pi B|\mathbf{w}|}{15v_\mathrm{F}}27\ \cos(2\theta+\phi). \tag{15}$$

Clearly, the tilt introduces an additional anisotropy in both the conductivity terms. In figure 3(a), we plot both the longitudinal and PH conductivities with the variation of the field angle θ for a fix tilt direction of $\phi = \pi/3$ and magnitude of $|\mathbf{w}| = 0.1$.

In figure 3(b) we plot the variation of both the longitudinal and PH conductivities with the variation of the tilt direction ϕ, for a fixed angle between electric and magnetic fields ($\theta = \pi/3$). Note that because of the sinusoidal dependence on ϕ, both current densities change sign, when the tilt direction is reversed, i.e., from ϕ to $(\phi + \pi)$. This behavior also matches with the analytical calculation in equation (12). Based on this, let us consider the PH current for different tilt configuration of the Dirac cone for a pair of WPs. Now, if, for a certain value of ϕ, the tilt for a pair of WPs is given by $\mathbf{w}_{\pm} = \pm\mathbf{w}$ then the Dirac cones are tilted towards each other. Then for $(\phi + \pi)$, the tilt vector for the pair becomes $\mathbf{w}_{\pm} = \mp\mathbf{w}$, i.e., the cones are tilted outwards in k-space (see figure 1(c) and (d)) and the direction of the PH current is reversed. This suggests that one can control the PH current via tilt engineering. For example, if the dispersion tilt can be controlled by some external parameters such as strain, then one can achieve strain-induced switching of the PH current or voltage due to the reversal of the relative tilt between the dispersion cones at the two WPs. An approach to generate and modulate the dispersion tilt in WSMs by means of rotational strain has been described in reference [48], where the chiral tilt varies to the linear order in the curl of the deformation vector (i.e., $\nabla \times \mathbf{u}$). By changing the direction of the applied rotational strain, one can therefore alter the sign of the tilt $\mathbf{w}_{\chi}$. In our theoretical analysis, we showed that the direction of PH current is dependent on the tilt direction, and hence, on the direction of the rotational strain. Thus, in an experimental set-up consisting of a WSM sample with PH measurement and where one can apply rotational strain to the sample, it could be possible to realize strain-induced switching of the PH current due to the tilt contribution.

The PHE in WSM has been addressed previously using the semiclassical approach in reference [33, 38] and recently by reference [49]. All these studies reveal the linear in B dependence of the PH conductivity which matches with our result. However, in these previous works, the direction and magnitude of the tilt have been fixed along a particular direction in the sample plane of the PH set-up. In a real WSM, however, the tilt direction is defined with respect to the crystallographic directions. Since the WSM samples can be prepared with different crystallographic orientations, it would be useful to investigate the effect of varying the tilt direction with respect to the PH measurement set-up, as was done in our study. We show that the variation in the tilt orientation adds a variable phase factor in the expression of the PH conductivity, and as a consequence the maximum and minimum values are shifted (figure 3(a)). Under this circumstance, the planar Hall current would be non-zero even when the electric and magnetic fields are parallel to each other. In addition, for a fixed angle between electric and magnetic fields, the longitudinal and PH currents are a function of the dispersion tilt (ϕ). The sinusoidal like dependence of the PH current on ϕ (figure 3(b)) confirms that its direction can be switched by changing only the tilt direction, an effect which has not been reported to the best of our knowledge.

Case (b). This case corresponds to the scenario where the tilt is uniform, i.e., when $\mathbf{w}_{\chi} = \mathbf{w}$ at all WPs. For this case, the current densities are given by, $\mathbf{j}^{(0)} = (8\pi/3)\sigma_0\mathbf{E}$, $\mathbf{j}^{(1)} = 0$, $\mathbf{j}^{(2)} = 2\pi\sigma_0 c_b^2(\frac{1}{3}(\mathbf{E}\cdot\mathbf{B})\mathbf{B} + \frac{1}{15}|\mathbf{B}|^2\mathbf{E})$. Specifically, in this case, the PH contribution from the two valleys would cancel out each other giving rise to zero net PH signal. The corresponding plots for the tilt dependence of the zeroth and second-order current densities are plotted in the supplemental.

Type-II. For the type-II WSMs ($|\mathbf{w}_{\chi}| > v_{\mathrm{F}}$) the FS is open and adopts a hyperboloid configuration. Since, by definition, we are in the large tilt regime, no simple analytical expressions of the current densities can be obtained. Instead, we perform numerical calculations of the conductance in type-II WSM from the integrations in equations (6)–(8) for different values of tilt parameter w_x (considering $\mathbf{w}_{\chi} = \chi\mathbf{w}$). These numerical results are plotted in the supplemental. Interestingly, we find similar trends in the current density compared to that of type-I WSM, e.g., the current densities tend to increase with the tilt strength. More importantly, the tilt-induced PH signal is still present in the case of type-II WSM.

IRS breaking WSM. In the above formulation we have considered TRS breaking WSMs where the WPs are separated in the momentum space. However, in the case of inversion symmetry (IRS) breaking WSMs, the WPs are separated along the energy axis. The corresponding Hamiltonian in the presence of chiral tilt is then given by $H_{\chi} = \chi v_{\mathrm{F}}\boldsymbol{\sigma}\cdot\mathbf{k} + \chi I Q_0/2 + I\chi\mathbf{w}\cdot\mathbf{k}$, where Q_0 is the separation between the WPs along the energy axis. In this case, the Fermi surface (FS) for the two opposite Weyl nodes would have different sizes and this difference is dependent on Q_0. As a consequence, our current density also changes with Q_0. In figure 4(a), we plot the longitudinal component of the $\mathbf{j}^{(1)}$ which increases non-linearly with Q_0 for an electric field applied along $\mathbf{E} \parallel (\hat{x} + \hat{y} + \hat{z})$. This increase with the Q_0 can be explained by considering the chiral contribution of the current density. For, $Q_0 = 0$, the size of the FS is same for the two chiral contributions and, as a consequence, after summing over the contributions coming from the opposite chiralities, all the terms which are proportional to the chirality would cancel out. However, for finite Q_0, since the size of the the FS is different the terms which are linear in chirality would still contribute, and these additional terms leads to the increase in the magnitude of the current density. In figure 4(b), we plot the longitudinal current density with the x-component of tilt (w_x) when $Q_0/\epsilon_{\mathrm{F}} = 0.1$. We see almost a

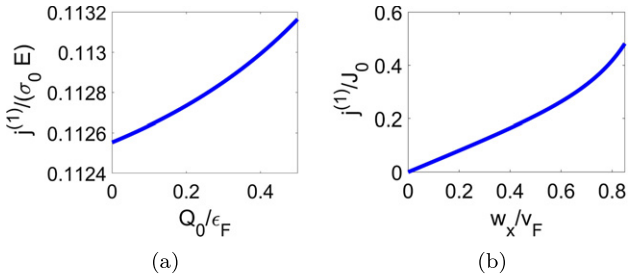

Figure 4. Plot of longitudinal component of $\mathbf{j}^{(1)}$ with respect to (a) the separation between the WPs along energy axis, Q_0 when $w_x = 0.2$ and, (b) the x-component of tilt (w_x) when $Q_0/\epsilon_F = 0.1$.

similar pattern for the TRS breaking case (figure 2), i.e., the current density increases linearly with the tilt magnitude but non-linearity occurs for large value of tilt unlike previous case. In the Supplemental, we have also plotted the variation of the longitudinal components of the zeroth $\mathbf{j}^{(0)}$ and second-order $\mathbf{j}^{(2)}$ contributions with Q_0, which show similar behavior as $\mathbf{j}^{(1)}$.

4. Conclusion

Using a semiclassical approach, we analyze the magnetotransport of a WSM with Dirac cones that are tilted in arbitrary directions in the momentum space. We derive the analytical expressions of the longitudinal and PH conductivity to the first order in tilt which agree with the numerical treatment done for arbitrary values of tilt. In addition, we evaluate the planar Hall (PH) current when the magnetic field, electric field, and the tilt vector lie in the same plane, and show that the direction of this current can be switched by modifying the tilt direction. A tilt-induced transverse current exists even when $\mathbf{E} \parallel \mathbf{B}$, where the conventional Hall current vanishes.

Acknowledgments

This work is supported by the following grants: MOE Tier I (NUS Grant No. R-263-000-D66-114), MOE Tier II MOE2018-T2-2-117 (NUS Grant No R-398-000-092-112), R-263-000-D61-114 (MOE Tier 1) and NRF-CRP12-2013-01 (NUS Grant No R-263-000-B30-281).

ORCID iDs

Anirban Kundu https://orcid.org/0000-0002-9780-9329
Zhuo Bin Siu https://orcid.org/0000-0002-7056-937X
Hyunsoo Yang https://orcid.org/0000-0003-0907-2898
Mansoor B A Jalil https://orcid.org/0000-0002-9513-8680

References

[1] Son D T and Yamamoto N 2013 Kinetic theory with berry curvature from quantum field theories *Phys. Rev.* D **87** 085016
[2] Murakami S 2007 Phase transition between the quantum spin Hall and insulator phases in 3d: emergence of a topological gapless phase *New J. Phys.* **9** 356
[3] Wan X, Turner A M, Vishwanath A and Savrasov S Y 2011 Topological semimetal and Fermi-arc surface states in the electronic structure of pyrochlore iridates *Phys. Rev.* B **83** 205101
[4] Armitage N P, Mele E J and Vishwanath A 2018 Weyl and dirac semimetals in three-dimensional solids *Rev. Mod. Phys.* **90** 015001
[5] Hasan M Z, Xu S-Y, Belopolski I and Huang S-M 2017 Discovery of Weyl Fermion semimetals and topological Fermi arc states *Ann. Rev. Condens. Matter Phys.* **8** 289–309
[6] Yan B and Felser C 2017 Topological materials: Weyl semimetals *Ann. Rev. Condens. Matter Phys.* **8** 337–54
[7] Nielsen H B and Ninomiya M 1983 The Adler–Bell–Jackiw anomaly and Weyl fermions in a crystal *Phys. Lett.* B **130** 389–96
[8] Spivak B Z and Andreev A V 2016 Magnetotransport phenomena related to the chiral anomaly in Weyl semimetals *Phys. Rev.* B **93** 085107
[9] Arnold F *et al* 2016 Negative magnetoresistance without well-defined chirality in the Weyl semimetal TaP *Nat. Commun.* **7** 11615
[10] Li C-Z, Wang L-X, Liu H, Wang J, Liao Z-M and Yu D-P 2015 Giant negative magnetoresistance induced by the chiral anomaly in individual Cd_3As_2 nanowires *Nat. Commun.* **6** 10137
[11] Li Q *et al* 2016 Chiral magnetic effect in ZrTe5 *Nat. Phys.* **12** 550

[12] Huang X *et al* 2015 Observation of the chiral-anomaly-induced negative magnetoresistance in 3d Weyl semimetal TaAs *Phys. Rev.* X **5** 031023
[13] Xiong J, Kushwaha S K, Tian L, Krizan J W, Hirschberger M, Wang W, Cava R J and Ong N P 2015 Evidence for the chiral anomaly in the Dirac semimetal Na_3Bi *Science* **350** 413–6
[14] Zhang C-L *et al* 2016 Signatures of the Adler–Bell–Jackiw chiral anomaly in a Weyl Fermion semimetal *Nat. Commun.* **7** 10735
[15] Gao Y, Yang S A and Niu Q 2017 Intrinsic relative magnetoconductivity of nonmagnetic metals *Phys. Rev.* B **95** 165135
[16] Goswami P, Pixley J H and Sarma S D 2015 Axial anomaly and longitudinal magnetoresistance of a generic three-dimensional metal *Phys. Rev.* B **92** 075205
[17] Goerbig M O, Fuchs J-N, Montambaux G and Piéchon F 2008 Tilted anisotropic Dirac cones in quinoid-type graphene and $\alpha-(BEDT\text{-}TTF)_2I_3$ *Phys. Rev.* B **78** 045415
[18] Soluyanov A A, Gresch D, Wang Z, Wu Q, Troyer M, Dai X and Bernevig B A 2015 Type-II Weyl semimetals *Nature* **527** 495
[19] Xu S-Y *et al* 2017 Discovery of Lorentz-violating type II Weyl Fermions in LaAlGe *Sci. Adv.* **3** e1603266
[20] Deng K *et al* 2016 Experimental observation of topological Fermi arcs in type-II Weyl semimetal MoTe2 *Nat. Phys.* **12** 1105
[21] Li P *et al* 2017 Evidence for topological type-II Weyl semimetal WTe2 *Nat. Commun.* **8** 2150
[22] McCormick T M, Kimchi I and Trivedi N 2017 Minimal models for topological Weyl semimetals *Phys. Rev.* B **95** 075133
[23] Yu Z-M, Yao Y and Yang S A 2016 Predicted unusual magnetoresponse in type-II Weyl semimetals *Phys. Rev. Lett.* **117** 077202
[24] O'Brien T E, Diez M and Beenakker C W J 2016 Magnetic breakdown and Klein tunneling in a type-II Weyl semimetal *Phys. Rev. Lett.* **116** 236401
[25] Zyuzin A A and Tiwari R P 2016 Intrinsic anomalous Hall effect in type-II Weyl semimetals *JETP Letters* **103** 717–22
[26] Wang Q *et al* 2019 Anomalous photothermoelectric transport due to anisotropic energy dispersion in WTe2 *Nano Lett.* **19** 2647–52
[27] He P *et al* 2019 Nonlinear magnetotransport shaped by Fermi surface topology and convexity *Nat. Commun.* **10** 1290
[28] Sharma G, Goswami P and Tewari S 2016 Nernst and magnetothermal conductivity in a lattice model of Weyl Fermions *Phys. Rev.* B **93** 035116
[29] Ferreiros Y, Zyuzin A A and Bardarson J H 2017 Anomalous Nernst and thermal Hall effects in tilted Weyl semimetals *Phys. Rev.* B **96** 115202
[30] Saha S and Tewari S 2018 Anomalous Nernst effect in type-II Weyl semimetals *Eur. Phys. J.* B **91** 4
[31] Mukherjee S P and Carbotte J P 2017 Absorption of circular polarized light in tilted type-I and type-II Weyl semimetals *Phys. Rev.* B **96** 085114
[32] Yesilyurt C, Siu Z B, Tan S G, Liang G and Jalil M B A 2017 Conductance modulation in Weyl semimetals with tilted energy dispersion without a band gap *J. Appl. Phys.* **121** 244303
[33] Ma D, Jiang H, Liu H and Xie X C 2019 Planar hall effect in tilted Weyl semimetals *Phys. Rev.* B **99** 115121
[34] Das K and Agarwal A 2019 Linear magnetochiral transport in tilted type-I and type-II Weyl semimetals *Phys. Rev.* B **99** 085405
[35] Rostamzadeh S, Adagideli İ and Goerbig M O 2019 Large enhancement of conductivity in Weyl semimetals with tilted cones: Pseudorelativity and linear response *Phys. Rev.* B **100** 075438
[36] Yesilyurt C, Siu Z B, Tan S G, Liang G, Yang S A and Jalil M B A 2017 Anomalous tunneling characteristic of Weyl semimetals with tilted energy dispersion *Appl. Phys. Lett.* **111** 063101
[37] Yesilyurt C, Siu Z B, Tan S G, Liang G, Yang S A and Jalil M B A 2019 Electrically tunable valley polarization in Weyl semimetals with tilted energy dispersion *Sci. Rep.* **9** 4480
[38] Nandy S, Sharma G, Taraphder A and Tewari S 2017 Chiral anomaly as the origin of the planar Hall effect in Weyl semimetals *Phys. Rev. Lett.* **119** 176804
[39] Kumar N, Guin S N, Felser C and Shekhar C 2018 Planar Hall effect in the Weyl semimetal GdPtBi *Phys. Rev.* B **98** 041103
[40] Son D T and Spivak B Z 2013 Chiral anomaly and classical negative magnetoresistance of Weyl metals *Phys. Rev.* B **88** 104412
[41] Sundaram G and Niu Q 1999 Wave-packet dynamics in slowly perturbed crystals: gradient corrections and berry-phase effects *Phys. Rev.* B **59** 14915–25
[42] Xiao D, Chang M-C and Niu Q 2010 Berry phase effects on electronic properties *Rev. Mod. Phys.* **82** 1959–2007
[43] Zyuzin V A 2017 Magnetotransport of Weyl semimetals due to the chiral anomaly *Phys. Rev.* B **95** 245128
[44] Lundgren R, Laurell P and Fiete G A 2014 Thermoelectric properties of Weyl and Dirac semimetals *Phys. Rev.* B **90** 165115
[45] Kim K-S, Kim H-J and Sasaki M 2014 Boltzmann equation approach to anomalous transport in a Weyl metal *Phys. Rev.* B **89** 195137
[46] Cortijo A 2016 Linear magnetochiral effect in Weyl semimetals *Phys. Rev.* B **94** 241105
[47] Huang S-M *et al* 2015 A Weyl fermion semimetal with surface Fermi arcs in the transition metal monopnictide TaAs class *Nat. Commun.* **6** 7373
[48] Vicente A and Vozmediano M A H 2018 Rotational strain in Weyl semimetals: a continuum approach *Phys. Rev.* B **97** 201404
[49] Ghosh S, Sinha D, Nandy S and Taraphder A 2019 Chirality-dependent planar Hall effect in inhomogeneous Weyl semimetals (arXiv 1911.01130)